

## Observing vortex polarization singularities at optical band degeneracies

Ang Chen,<sup>1,3</sup> Wenzhe Liu,<sup>1,3</sup> Yiwen Zhang,<sup>1,3</sup> Bo Wang,<sup>1,3</sup> Xiaohan Liu,<sup>1,3</sup> Lei Shi,<sup>1,3,\*</sup> Ling Lu,<sup>2</sup> and Jian Zi<sup>1,3,†</sup>

<sup>1</sup>*Department of Physics, Key Laboratory of Micro- and Nano-Photonic Structures (Ministry of Education), and State Key Laboratory of Surface Physics, Fudan University, Shanghai 200433, China*

<sup>2</sup>*Institute of Physics, Chinese Academy of Sciences/Beijing National Laboratory for Condensed Matter Physics, Beijing 100190, China*

<sup>3</sup>*Collaborative Innovation Center of Advanced Microstructures, Fudan University, Shanghai 200433, China*



(Received 13 December 2018; published 6 May 2019)

In the momentum space of two-dimensional (2D) periodic photonic systems, the polarization states of radiating Bloch modes on a single band can form vortex polarization singularities. Here, we study vortex polarization singularities at the band degeneracies. We design a quadratic degeneracy in a plasmonic crystal with  $C_{4v}$  symmetry which, by symmetry breaking, splits into a pair of Dirac points with half vortices. The integer vortex singularity at the quadratic degeneracy and the half one at the Dirac degeneracy are measured using polarization-resolved momentum-space imaging spectroscopy. The complete evolution of the splitting from the integer vortex to a pair of half vortices is observed in experiments.

DOI: [10.1103/PhysRevB.99.180101](https://doi.org/10.1103/PhysRevB.99.180101)

Electromagnetic (EM) waves in free space are transverse waves and their polarization states are defined as the orbits of their oscillating electric vectors. For a monochromatic electromagnetic wave, polarization states can be position varying and form interesting geometries with polarization singularities [1–3]. Polarization singularities robustly exist and have been researched for years in light beams and near fields of micro- and nanostructures [4–8]. One type is the vortex polarization singularity (or V point) [9–11]. The field intensity at the vortex singularity vanishes, and the main axis of the polarization states winds around. Beams with such singularities find applications in focusing and imaging [12–14]. In the momentum space of two-dimensional (2D) periodic systems, vortex polarization singularities are as well found at specific locations of the Brillouin zone (BZ) along the bands [15–19]. The vortices of integer charges at nondegenerate states are analyzed and observed in photonic and plasmonic systems [15–18]. The singular polarization states as the centers of these vortices lead to interesting phenomena such as bound states in the continuum (BICs) [15–18,20] and can be applied in vector beam generation [21]. Meanwhile, half vortices are discovered around the bulk Fermi arcs resulting from non-Hermiticity and are spawned from Dirac degeneracies [19]. The charges (or Poincaré-Hopf indices) of the on-band momentum-space vortex singularities are believed to be linked with the topological properties of the band structure. Since degeneracies are more important than singlets in topological photonics and the lifting of degeneracies is closely linked with topological transportation phenomena [22], vortex polarization singularities at the band degeneracies are worth studying. It will enable a direct observation of the topological properties of photonic bands, and can inspire works studying topological band inversion from a different perspective.

Moreover, the superposition of vortex singularities at the band degeneracies brings forward more room to control the radiation. In this Rapid Communication, we research vortex polarization singularities at the band degeneracies. The topological link between the degeneracy type and the on-band vortex singularity is explained. We show theoretically and experimentally that there is an integer vortex singularity at the quadratic degeneracy that, with symmetry breaking, breaks into a pair of half ones associated with the Dirac points.

Degeneracies in 2D systems are classified into two categories according to the dispersions in the vicinity, quadratic degeneracy points and linear degeneracy points (Dirac points), as shown in Fig. 1. The two kinds of degeneracies are topologically different according to their Berry phases, which is an extra phase the wave function acquires over a cycle evolution of Bloch states. Berry phases of the quadratic degeneracy points are trivial ( $0$  or  $2\pi$ ), while those of the Dirac points are nontrivial ( $\pi$ ) [23–25]. The trivial Berry phase around the quadratic degeneracy makes the allowed charges of the corresponding vortex polarization singularities the same as the nondegenerate cases, which have integer charges (the schematic view shown in the left panel of Fig. 1). On the contrary, the nontrivial Berry flux at the Dirac point allows the existence of half-integer vortices. With a closed loop around the Dirac point, the wave function of the Bloch mode would gain a  $\pi$  geometric phase. Thus, the main axis of the polarization state would only need to turn  $(2n + 1)\pi$  in the direction to return to itself after tracing the loop, resulting in half-integer vortices [19]. See the right panel of Fig. 1 for a lowest-order ( $-1/2$ ) example. As is complementary, accidental Dirac points previously studied [26–28] are usually composed of a topologically trivial quadratic degeneracy and a topologically trivial singlet, indicating that the polarization singularities at the accidental degeneracies have no difference from the composing modes. Results on the accidental case are shown in the Supplemental Material (SM) [29]. Note that the systems we study in this Rapid Communication all

\*lshi@fudan.edu.cn

†jzi@fudan.edu.cn

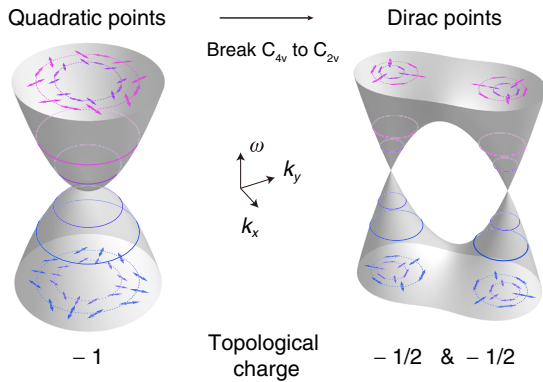


FIG. 1. Band degeneracies and vortex polarization singularities (lowest order). A quadratic degeneracy can be split into two Dirac points. The configuration of polarization states in the vicinity of the two types of band degeneracies is shown.

have  $C_2$  symmetry, which makes the polarization states in our systems almost linear [30]. There would also be pure linear polarization states at specific positions in the BZ guaranteed by the mirror symmetry of the systems. For convenience, we will only plot the major axis (polarization azimuths) of the polarization states here. The information on the ellipticity of the polarization states is included in the SM [29].

In order to study such on-band vortex singularities and to seek the link between half and integer ones at the degeneracies, a plasmonic crystal is applied. It is a periodically corrugated poly(methyl methacrylate) (PMMA) layer on a flat silver substrate [31]. Due to the periodic perturbation induced by the air hole arrays, the propagating surface plasmon polaritons (SPPs) could be excited with a plane wave, forming well-defined band structures. If the system has specific symmetries ( $C_{4v}$  or  $C_{6v}$ ), a pair of bands can be degenerate quadratically at a high-symmetry point, such as the center ( $\Gamma$  point) of the first BZ. This quadratic degeneracy can be further regarded as a pair of linear degeneracies continuable to the Dirac points, which can be obtained by symmetry breaking [32,33], as shown in Fig. 1. Here, we took this method to observe the evolution from a quadratic degeneracy point splitting into a pair of linear degeneracy points. The corresponding integer vortex splitting into pairs of half vortices is also shown. The sum of those half vortices after symmetry breaking equals that of integer vortices, approving the law of charge conservation.

The band structures along the  $\Gamma$ - $M$  direction and the corresponding polarization azimuths of both kinds of degeneracies are calculated by using a finite-element method (COMSOL MULTIPHYSICS), as shown in Fig. 2. The structures studied are illustrated in Fig. 2(a). The silver substrates are 200 nm thick, ensuring that there is no light transmitted. The thickness of PMMA is 80 nm, and the period ( $a$ ) of square arrays of rectangular air holes is 600 nm. The length-width ratio  $l/w$  ( $l$ ,  $w$  are the length and width of a rectangle hole, respectively, and the direction of  $l$  is along the diagonal lines of the square lattice) of air holes equals 1 and 1.48, respectively, in the left and right panels of Fig. 2. In the left panel of Fig. 2(a), when  $l/w = 1$ , the upper and lower bands are quadratically degenerate at the  $\Gamma$  point, which is protected by  $C_{4v}$  symmetry. The corresponding polarization azimuths calculated from

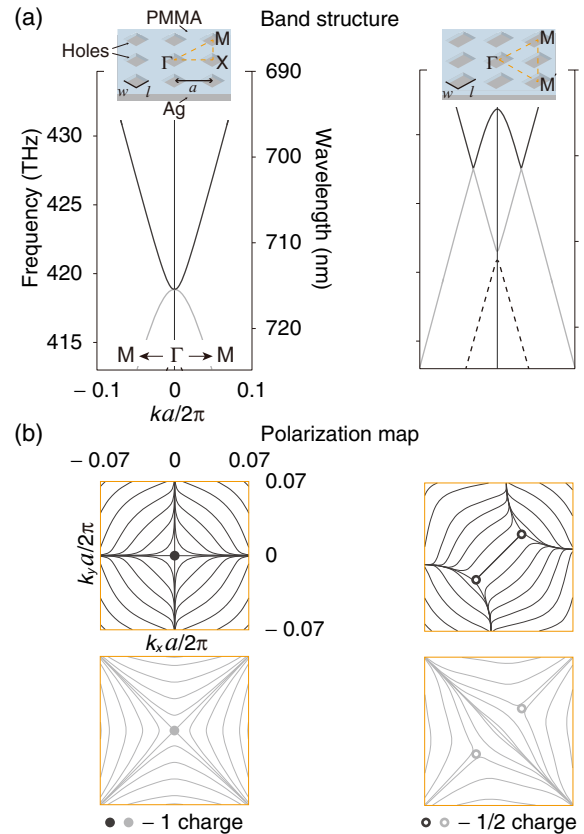


FIG. 2. (a) Band structures and (b) the corresponding polarization azimuth maps (lower panel) of quadratic and linear degeneracies in the form of streamlines. The bands of interest are denoted by solid lines, while the others by dashed lines. Left: In a plasmonic structure with  $C_{4v}$  symmetry, a pair of bands can be degenerate quadratically at the  $\Gamma$  point. Right: In the  $C_{2v}$ -symmetric structure, a pair of bands can be degenerate linearly along the high-symmetry line (here, the  $\Gamma$ - $M$  direction).

far-field radiation in a small region of the first BZ near the  $\Gamma$  point are shown in the left panel of Fig. 2(b) for both bands. Tracing counterclockwise loops around the  $\Gamma$  point, we are able to see that the azimuths on both bands have a  $-2\pi$  change, which means that the vortex singularities at the  $\Gamma$  point are both of  $-1$  charges.

When the length of the rectangle hole is increased to  $l/w = 1.48$  (all other parameters fixed) in the right panel, the symmetry reduces to  $C_{2v}$ . Consequently, the quadratic degeneracy protected by  $C_{4v}$  splits into a pair of Dirac cones along the  $\Gamma$ - $M$  direction which has  $C_{1v}$  symmetry. From the calculated polarization distributions shown below, it is found that the vortex singularity of  $-1$  disappears at the  $\Gamma$  point and a pair of vortex singularities appear along  $\Gamma$ - $M$  corresponding to the Dirac points. The polarization azimuth is parallel to itself after a closed loop around one Dirac point with a winding angle  $-\pi$ , showing that the vortex singularities at the Dirac points are half ones. The same results are also observed in the case of reducing the  $C_{6v}$  symmetry of the hexagonal lattice, shown in the SM [29]. In general, this phenomenon proved that the topological behavior in polarization fields defined on the bands is closely linked to the symmetry.

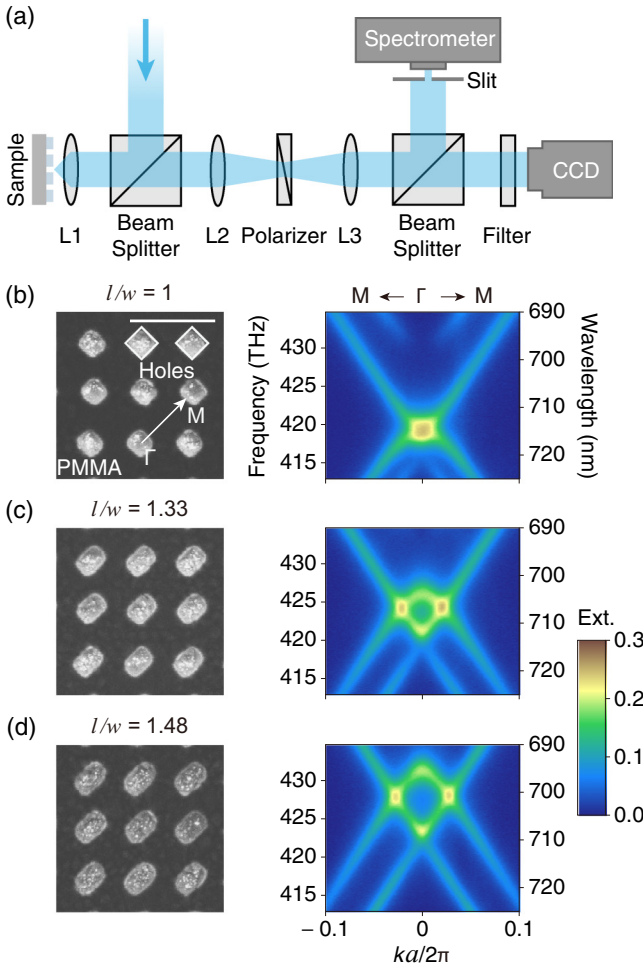


FIG. 3. (a) Experimental setup of the home-made momentum-space imaging spectroscopy based on Fourier transformation. The real-space spectral information is transformed into momentum-space information after the light passing the objective lens (L1). A polarizer is located in the plane conjugate to the sample plane to obtain polarization-dependent information. Meanwhile, a spectrometer and a CCD are put in the planes conjugate to the back focal plane of the objective lens to get Fourier-transformed spectra and isofrequency contours. L2, L3: Fourier transform lenses. (b)–(d) The SEM images of the plasmonic structures and experimentally measured band structures (extinction spectra) along the  $\Gamma$ - $M$  direction. From top to bottom, the width ( $w$ ) of the holes stays the same,  $w = 290$  nm, while the length  $l$  increases,  $l = 290, 385, 430$  nm. The white scale bars:  $1 \mu\text{m}$ . (b)  $l/w = 1$  corresponds to  $C_{4v}$  symmetry. A quadratic degeneracy point appears at the  $\Gamma$  point. (c)  $l/w = 1.33$  and (d)  $l/w = 1.48$  correspond to  $C_{2v}$  symmetry.

To experimentally verify the above discussions, we fabricated a series of samples with different  $l/w$  using electron beam lithography. A 200-nm-thick silver substrate layer is coated onto a slide by thermal evaporation, which is thick enough to block any light transmission. Then, a PMMA layer is spin coated onto the substrate. Using electron beam lithography, the designed hole arrays are then etched on the PMMA layer. The scanning electron microscopy (SEM) images of the samples with different ratios  $l/w$  are shown in the left panel of Figs. 3(b)–3(d). Subsequently, we measured the angle

( $k$ )-resolved extinction spectra (one minus reflectivity) of the samples as a function of frequencies and wave vectors, applying our home-made momentum-space imaging spectroscopy based on optical Fourier transformation. The instrumental setup is illustrated in Fig. 3(a), while the working principle is detailed in a previous work [17]. Since the system has no transmission, Fano resonance and Fabry-Pérot features in the spectrum disturbing the observation in the previous works [15, 18] will be prevented, and the extinction (or absorption) will directly reflect the far-field polarization property of the eigenmodes [17]. As shown in the right panel of Figs. 3(b)–3(d), the band structures along the  $\Gamma$ - $M$  direction can be obtained from the peaks of the extinction spectra. When  $l/w = 1$ , the quadratic degeneracy at the  $\Gamma$  point is protected by the  $C_{4v}$  symmetry of the structure and thus there is only one peak of the extinction spectra in the wavelength range of interest; see Fig. 3(b). When  $l/w \neq 1$ , the  $C_{4v}$  symmetry of the structures is broken to  $C_{2v}$ . At the  $k = 0$  point, there are two extinction maxima instead of one maximum in the  $C_{4v}$  case. Meanwhile, we can find two linear dispersion emerge along  $\Gamma$ - $M$ , i.e., Dirac points, as shown in Figs. 3(c) and 3(d). When  $l/w = 1.33$ , the Dirac points whose wavelength is 706 nm appear at the wave vector  $k_{\parallel} = \pm 0.023 \times 2\pi/a$  along  $\Gamma$ - $M$ . As  $l/w$  becomes larger ( $l/w = 1.48$ ), the Dirac points will move outwards along  $\Gamma$ - $M$  and appear at  $k_{\parallel} = \pm 0.027 \times 2\pi/a$ , with the wavelength 702 nm. The experimental results along the  $\Gamma$ - $M$  direction agree well with theoretical ones (Fig. 2). The experimental data along other directions are provided in the SM [29].

For a direct observation on the vortex singularities at the band degeneracies, we measured the polarization-resolved isofrequency contours as a map of extinction and summed them with a range of wavelengths [17]. The summed polarization-resolved isofrequency contour spans a spectral range and can show the topological property of the band from a polarization point of view. In addition, the individual isofrequency contours at single frequencies are shown in the SM [29]. In Fig. 4, we plotted the summed isofrequency contours of the lower bands of the  $C_{4v}$ -symmetric structure ( $l/w = 1$ ) and  $C_{2v}$ -symmetric structure ( $l/w = 1.48$ ), as shown in Figs. 4(a) and 4(b), respectively. The center one is measured under unpolarized illumination, while the ones outside are polarization resolved. Polarization-resolved extinction of the plasmonic crystal is directly related to the polarization states of the eigenmodes [17], thus our system is a powerful platform studying the polarization field in the momentum space. With  $C_2$  symmetry, the polarization states of Bloch states in our system are nearly linear, as we mentioned [30]. Thus, when the far-field polarization azimuths of certain states are perpendicular to the polarizer, the signal at such points will almost diminish in the polarization-resolved plots, appearing as dark areas.

Hence, these vortex singularities can be viewed as rotating dark patterns along with the polarizer in summed isofrequency contours, which gives a vivid picture of winding polarization azimuths. The shape, spinning speed, and spinning direction of such patterns directly reveal the sign and magnitude of the charges carried by the vortices. For the  $C_{4v}$ -symmetric structure, we can see that there is one dark strip spinning around the  $\Gamma$  point. The strip rotates  $\pi$  clockwise when the polarizer

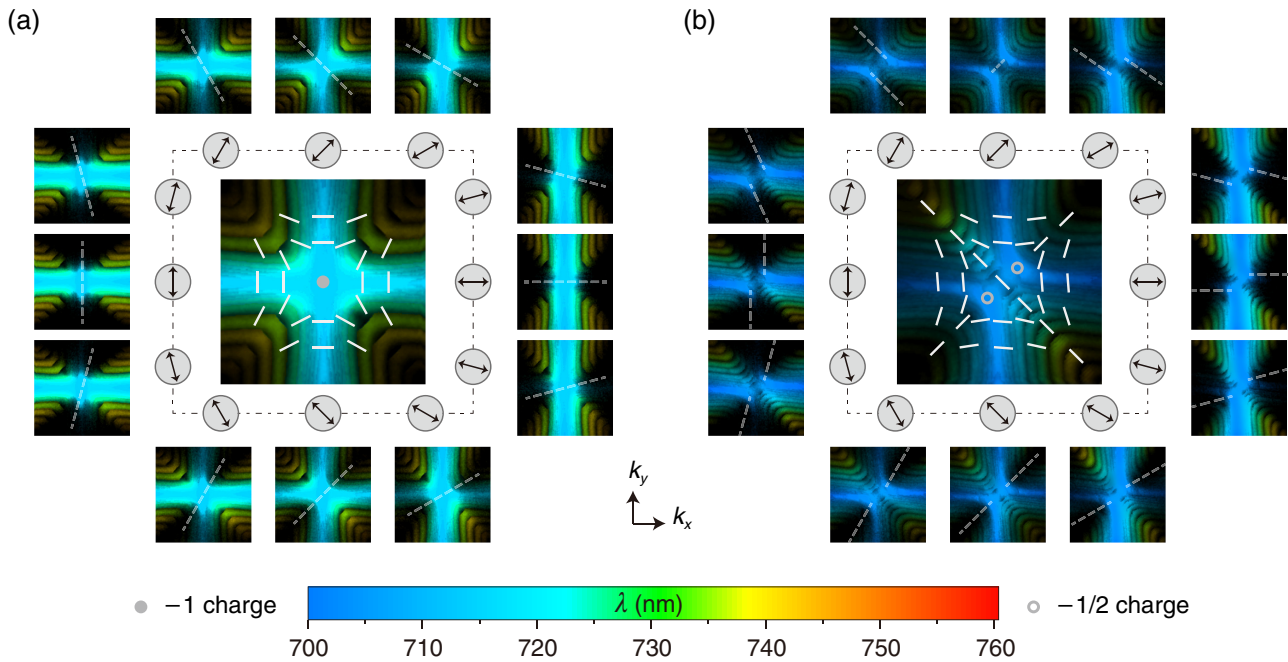


FIG. 4. Extinction map of the band of interest in the BZ, obtained by summing 12 isofrequency contours. Central plot: Unpolarized extinction map. Side plots: Polarization-resolved extinction maps. The arrows aside indicate the direction of the polarizer. Different colors correspond to different wavelengths, with the color map shown beside. The centers of integer and half-vortex singularities are marked by solid and open dots in the unpolarized plot. Measured polarization azimuth configurations of those vortices are sampled around vortex centers. (a)  $C_{4v}$ -symmetric system,  $l/w = 1$ . (b)  $C_{2v}$ -symmetric system,  $l/w = 1.48$ .

rotates  $\pi$  counterclockwise, indicating the charge of the degeneracy point is  $-1$ . Note that the state at the degeneracy point is always excited under arbitrary polarization, rather than a BIC, thus making the vortex center always bright and the dark strip appearing disconnected. Such a singular polarization state resulting from the superposition of two polarization singularities at the quadratic degeneracy would be applicable in freely controlling the emitted polarization.

As for the  $C_{2v}$ -symmetric structure, there are two spinning dark radials rather than one strip in the  $C_{4v}$  case. The state at the  $\Gamma$  point can be either excited or not under different polarizations, which is distinguished from the degenerate state of  $C_{4v}$  symmetry. On the other hand, the vortex centers at the Dirac points are always excited rather than forming bound states in the continuum. The radials in  $C_{2v}$  system rotate  $2\pi$  clockwise when the polarizer rotates  $\pi$  counterclockwise, showing the charges here are both  $-1/2$ . Two animations showing those spinning patterns are present in the SM [29]. For an intuitive understanding, we give a schematic view of the spinning dark patterns for the half vortices; see the SM [29]. The distributions of polarization azimuths forming vortices are obtained and plotted in the central figure, and vortex centers are shown. The results agree well with our theory. Evidently when symmetry of the structure is changed from  $C_{4v}$  to  $C_{2v}$ , the  $-1$  charge at the quadratic degeneracy point splits into two  $-1/2$  charges at the linear degeneracy points, approving charge conservation. The phenomenon is linked to the separation of polarization singularities when symmetry is broken [8].

In summary, we showed theoretically and experimentally the existence of integer vortex singularities at quadratic band degeneracies and half ones at Dirac points in the momentum space of the plasmonic structures. Via controlling the symmetry of the structure, the evolution from one quadratic degeneracy point to a pair of linear degeneracy points is clearly exhibited with the integer vortex singularities splitting into the half ones, which is consistent with charge conservation. These unique vortex singularities at the band degeneracies enrich the various topological phenomena in photonics, establishing a link between topological properties and polarization singularities [34–42]. They can accessibly enable half vector-vortex beams [43,44] or even lasers [21,45–47]. These findings also show great potential in polarization manipulation with photonic/plasmonic crystals by polarization. In the meantime, our plasmonic crystal structure will be a powerful platform to study the polarization feature in photonic band structures.

We thank Chia Wei Hsu, Yihua Wang, and Shaoyu Yin for helpful discussions. The work was supported by 973 Program and China National Key Basic Research Program (2015CB659400, 2016YFA0301100, 2016YFA0302000, and 2018YFA0306201) and National Science Foundation of China (11774063, 11727811, 91750102, and 11604355). The research of L.S. was further supported by Science and Technology Commission of Shanghai Municipality (17ZR1442300, 17142200100).

A.C., W.L., and Y.Z. contributed equally to this work.

- [1] J. Nye and J. Hajnal, *Proc. R. Soc. London, Ser. A* **409**, 21 (1987).
- [2] M. Dennis, *Opt. Commun.* **213**, 201 (2002).
- [3] K. Y. Bliokh, M. A. Alonso, and M. R. Dennis, [arXiv:1903.01304](https://arxiv.org/abs/1903.01304).
- [4] M. Burreli, R. J. P. Engelen, A. Opheij, D. van Oosten, D. Mori, T. Baba, and L. Kuipers, *Phys. Rev. Lett.* **102**, 033902 (2009).
- [5] B. Le Feber, N. Rotenberg, and L. Kuipers, *Nat. Commun.* **6**, 6695 (2015).
- [6] A. de Hoogh, L. Kuipers, T. Visser, and N. Rotenberg, *Photonics* **2**, 553 (2015).
- [7] R. Coles, D. Price, J. Dixon, B. Royall, E. Clarke, P. Kok, M. Skolnick, A. Fox, and M. Makhonin, *Nat. Commun.* **7**, 11183 (2016).
- [8] E. Ostrovsky, K. Cohen, S. Tsesses, B. Gjonaj, and G. Bartal, *Optica* **5**, 283 (2018).
- [9] I. Freund, *Opt. Commun.* **201**, 251 (2002).
- [10] R. W. Schoonover and T. D. Visser, *Opt. Express* **14**, 5733 (2006).
- [11] Ruchi, S. K. Pal, and P. Senthilkumar, *Opt. Express* **25**, 19326 (2017).
- [12] R. Dorn, S. Quabis, and G. Leuchs, *Phys. Rev. Lett.* **91**, 233901 (2003).
- [13] D. Biss and T. Brown, *Opt. Lett.* **28**, 923 (2003).
- [14] S. Carrasco, B. E. Saleh, M. C. Teich, and J. T. Fourkas, *J. Opt. Soc. Am. B* **23**, 2134 (2006).
- [15] C. W. Hsu, B. Zhen, J. Lee, S.-L. Chua, S. G. Johnson, J. D. Joannopoulos, and M. Soljačić, *Nature (London)* **499**, 188 (2013).
- [16] B. Zhen, C. W. Hsu, L. Lu, A. D. Stone, and M. Soljačić, *Phys. Rev. Lett.* **113**, 257401 (2014).
- [17] Y. Zhang, A. Chen, W. Liu, C. W. Hsu, B. Wang, F. Guan, X. Liu, L. Shi, L. Lu, and J. Zi, *Phys. Rev. Lett.* **120**, 186103 (2018).
- [18] H. M. Doeleman, F. Monticone, W. Hollander, A. Alù, and A. F. Koenderink, *Nat. Photonics* **12**, 397 (2018).
- [19] H. Zhou, C. Peng, Y. Yoon, C. W. Hsu, K. A. Nelson, L. Fu, J. D. Joannopoulos, M. Soljačić, and B. Zhen, *Science* **359**, 1009 (2018).
- [20] C. W. Hsu, B. Zhen, A. D. Stone, J. D. Joannopoulos, and M. Soljačić, *Nat. Rev. Mater.* **1**, 16048 (2016).
- [21] A. Kodigala, T. Lepetit, Q. Gu, B. Bahari, Y. Fainman, and B. Kanté, *Nature (London)* **541**, 196 (2017).
- [22] Z. Wang, Y. D. Chong, J. D. Joannopoulos, and M. Soljačić, *Phys. Rev. Lett.* **100**, 013905 (2008).
- [23] Y. Zhang, Y.-W. Tan, H. L. Stormer, and P. Kim, *Nature (London)* **438**, 201 (2005).
- [24] A. K. Geim and K. S. Novoselov, *Nat. Mater.* **6**, 183 (2007).
- [25] F. D. M. Haldane and S. Raghu, *Phys. Rev. Lett.* **100**, 013904 (2008).
- [26] X. Huang, Y. Lai, Z. H. Hang, H. Zheng, and C. T. Chan, *Nat. Mater.* **10**, 582 (2011).
- [27] K. Sakoda, *Opt. Express* **20**, 25181 (2012).
- [28] B. Zhen, C. W. Hsu, Y. Igarashi, L. Lu, I. Kaminer, A. Pick, S.-L. Chua, J. D. Joannopoulos, and M. Soljačić, *Nature* **525**, 354 (2015).
- [29] See Supplemental Material at <http://link.aps.org/supplemental/10.1103/PhysRevB.99.180101> for animations, notes and figures about (1) direct observation of polarization singularities at band degeneracies, (2) ellipticity map in the vicinity of Dirac point, (3) an alternative way to generate Dirac points and half vortices by squeezing the lattice, (4) polarization maps in a  $C_{6v}$  system and the corresponding symmetry broken case, (5) 3D plots of measured band structures, (6) measured isofrequency contours, (7) schematic view of polarization dependent extinction maps, and (8) results on an accidental degenerate case.
- [30] C. W. Hsu, B. Zhen, M. Soljačić, and A. D. Stone, [arXiv:1708.02197](https://arxiv.org/abs/1708.02197).
- [31] D. Han, F. Wu, X. Li, C. Xu, X. Liu, and J. Zi, *Appl. Rev. Lett.* **89**, 091104 (2006).
- [32] Y. D. Chong, X.-G. Wen, and M. Soljačić, *Phys. Rev. B* **77**, 235125 (2008).
- [33] H. Zhou, Tailoring light with photonic crystal slabs: From directional emission to topological half charges, Ph.D. thesis, Massachusetts Institute of Technology, 2016 .
- [34] L. Lu, J. D. Joannopoulos, and M. Soljačić, *Nat. Photonics* **8**, 821 (2014).
- [35] M. Xiao, Z. Q. Zhang, and C. T. Chan, *Phys. Rev. X* **4**, 021017 (2014).
- [36] W. Gao, M. Lawrence, B. Yang, F. Liu, F. Fang, B. Béri, J. Li, and S. Zhang, *Phys. Rev. Lett.* **114**, 037402 (2015).
- [37] D. Leykam and Y. D. Chong, *Phys. Rev. Lett.* **117**, 143901 (2016).
- [38] D. Leykam, M. C. Rechtsman, and Y. D. Chong, *Phys. Rev. Lett.* **117**, 013902 (2016).
- [39] C. He, X.-C. Sun, X.-P. Liu, M.-H. Lu, Y. Chen, L. Feng, and Y.-F. Chen, *Proc. Natl. Acad. Sci. U.S.A.* **113**, 4924 (2016).
- [40] Q. Wang, M. Xiao, H. Liu, S. Zhu, and C. T. Chan, *Phys. Rev. X* **7**, 031032 (2017).
- [41] Q. Guo, B. Yang, L. Xia, W. Gao, H. Liu, J. Chen, Y. Xiang, and S. Zhang, *Phys. Rev. Lett.* **119**, 213901 (2017).
- [42] Y. Guo, M. Xiao, and S. Fan, *Phys. Rev. Lett.* **119**, 167401 (2017).
- [43] A. M. Yao and M. J. Padgett, *Adv. Opt. Photonics* **3**, 161 (2011).
- [44] T. Bauer, P. Banzer, E. Karimi, S. Orlov, A. Rubano, L. Marrucci, E. Santamato, R. W. Boyd, and G. Leuchs, *Science* **347**, 964 (2015).
- [45] S. Noda, M. Yokoyama, M. Imada, A. Chutinan, and M. Mochizuki, *Science* **293**, 1123 (2001).
- [46] S. Iwahashi, Y. Kurosaka, K. Sakai, K. Kitamura, N. Takayama, and S. Noda, *Opt. Express* **19**, 11963 (2011).
- [47] B. Bahari, A. Ndao, F. Vallini, A. E. Amili, Y. Fainman, and B. Kanté, *Science* **358**, 636 (2017).

# Observing polarization vortices at optical band degeneracies: supplementary material

## 1 Supplementary Animations

(a)

(b)

(c)

(d)

Animation S1: Direct experimental observations of integer ( $-1$ ) and half ( $-1/2$ ) vortices in the momentum space for quadratic degeneracy [(a) with and (c) without mark lines] and linear/Dirac degeneracy [(b) with and (d) without mark lines]. (One should use Acrobat Reader to view these animations.)

## 2 Supplementary Notes

First of all, we calculated the ellipticity (the third Stokes parameter,  $S_3$ ) map of the lower band in our  $C_{2v}$  system. The maximum ellipticity in our system is approximately  $\pm 0.14$ . Due to the fact that our system possesses  $C_2$  symmetry, the polarization states are nearly linear, as shown in Figure S1.

In Figure S2, we show an alternative method to break the  $C_{4v}$  symmetry of the system into  $C_{2v}$ . Instead of stretching the shape of holes, we squeeze the lattice in the diagonal direction. One diagonal is unchanged, and the other is shortened. The angle between the unchanged diagonal and the side is reduced from  $45^\circ$  to  $41^\circ$ . The simulated band structure and the corresponding polarization maps are shown.

In Figure S3, we discuss the band degeneracies in the plasmonic structures of hexagonal lattice. The quadratic degeneracies are obtained at  $\Gamma$  point protected by  $C_{6v}$ -symmetry, and Dirac degeneracies are obtained around  $\Gamma$  point via breaking the  $C_{6v}$  to  $C_{2v}$ . From the maps of polarization vectors near  $\Gamma$  point, we show that the quadratic degeneracy points at  $\Gamma$  point correspond to topological charges of  $-2$ . And when the air holes are stretched along  $\Gamma$ -M, a pair of  $-1/2$  charges appear along this direction, with one  $-1$  charge fixed at  $\Gamma$  point.

Next we come back to the experimental data for the square lattice. In Figure S4, we plotted the measured three-dimensional band structures to clearly show the evolution from a quadratic degeneracy to a pair of linear/Dirac degeneracies. Figure S5 gives some examples of measured iso-frequency contours under narrow-band illumination with specific wavelengths for both  $C_{4v}$  and  $C_{2v}$  structures. By summing up these contours with a range of wavelengths, we can obtain the maps in Figure 4 of the main text.

To mimic the extinction maps of the experiment, we use some vector-field functions to show the polarization distributions and dark strips when rotating the polarizer, as shown in Figure S6.

Finally, we supplement our discussion on degeneracies with the accidental case. Here we take similar structures as in our main text. Choosing the holes to be square, the structures here have  $C_{4v}$  symmetry. The period is chosen to be 600 nm, and we tuned the widths of the squares from 395 nm to 406 nm, and then 415 nm. The gap between TM2 and TM3/TM4 would gradually close when the side length increases. When the side length becomes 406 nm, the three bands accidentally degenerate, and the degeneracy point turns out to be a Dirac point. Then the gap will open again with the increasing length. The corresponding band structures and polarization maps could be found in Figure S7. We find that the vortex polarization singularities on the three bands remain unchanged.

## 3 Supplementary Figures

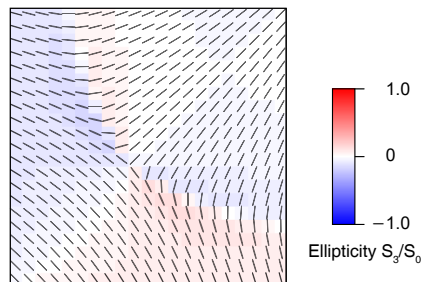


Figure S1: Calculated polarization map around the Dirac point of the lower band in our  $C_{2v}$  system. The polarization states are shown as the ellipses, while the ellipticities are shown as the color map.

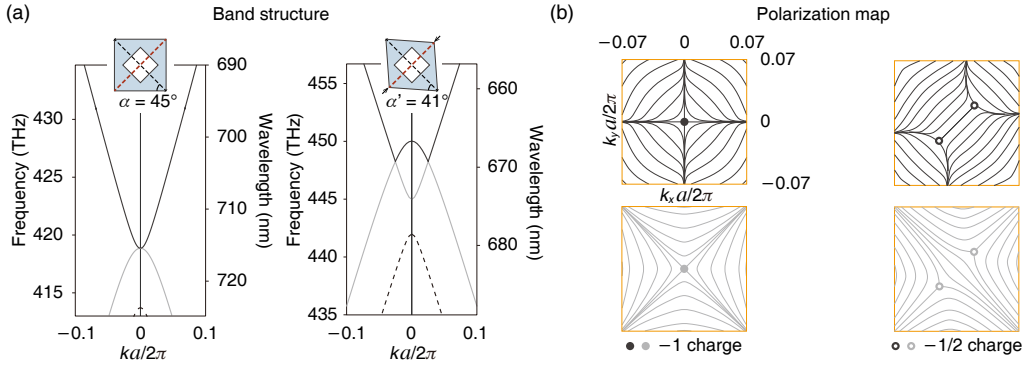


Figure S2: Calculated polarization map around the Dirac point of the lower band in our  $C_{2v}$  system. The polarization states are shown as the ellipses, while the ellipticities are shown as the color map.

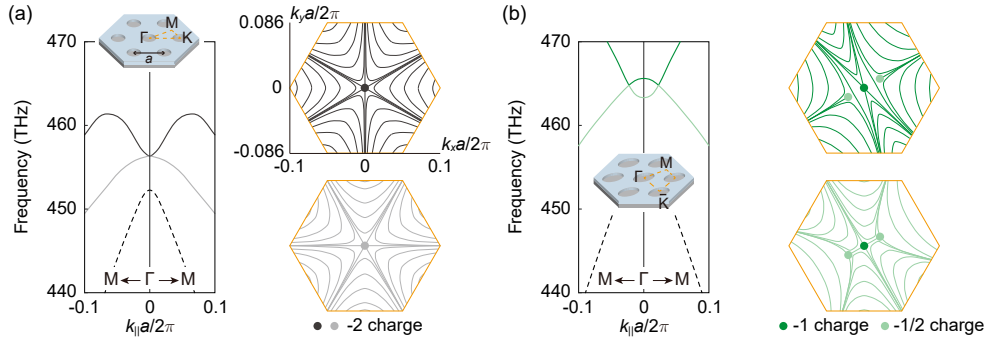


Figure S3: Band structures (left panel) and the corresponding polarization maps (right panel) of quadratic and linear degeneracies in hexagonal lattice. The bands of interest are denoted by solid lines, while others by dashed lines. (a) A pair of bands can be degenerate quadratically at  $\Gamma$  point protected by  $C_{6v}$  symmetry. (b) In the  $C_{2v}$ -symmetry structure, a pair of bands can be degenerate linearly along  $\Gamma$ -M direction.

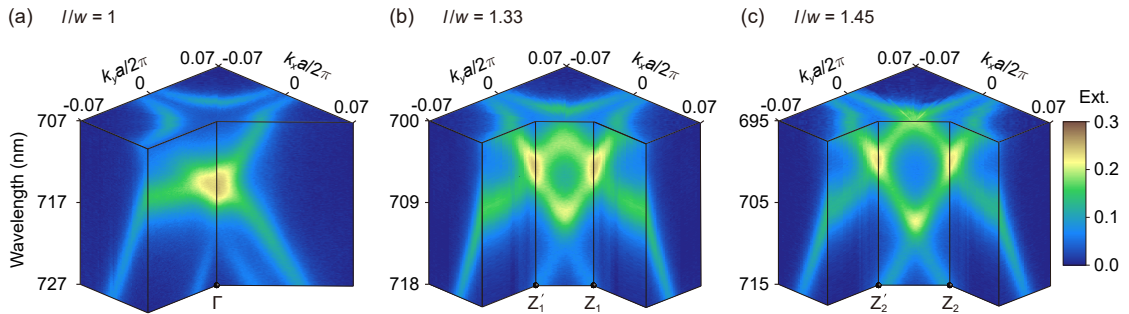


Figure S4: The measured three-dimensional (3D) band structures (extinction spectra) clearly show the evolution from a quadratic degeneracy point to a pair of Dirac degeneracy points. (a)  $l/w = 1$ . (b)  $l/w = 1.33$ . (c)  $l/w = 1.45$ .

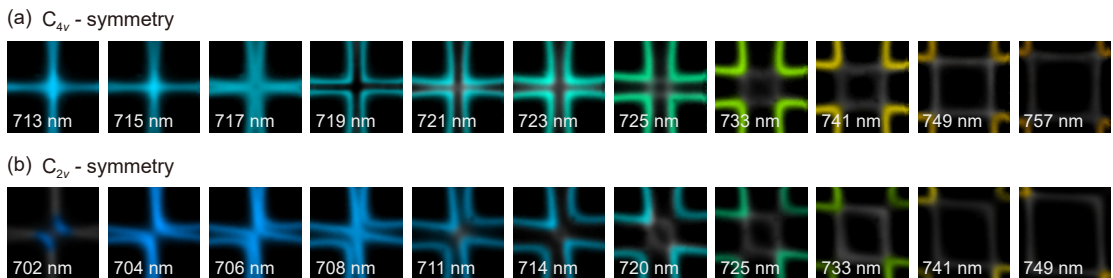


Figure S5: Measured iso-frequency contours of the plasmonic structures in square lattices under narrow-band illumination. Bands of interest are marked in colors. Different colors correspond to different wavelengths shown aside. (a)  $C_{4v}$ -symmetry structure,  $l/w = 1$ . (b)  $C_{2v}$ -symmetry structure,  $l/w = 1.48$ .

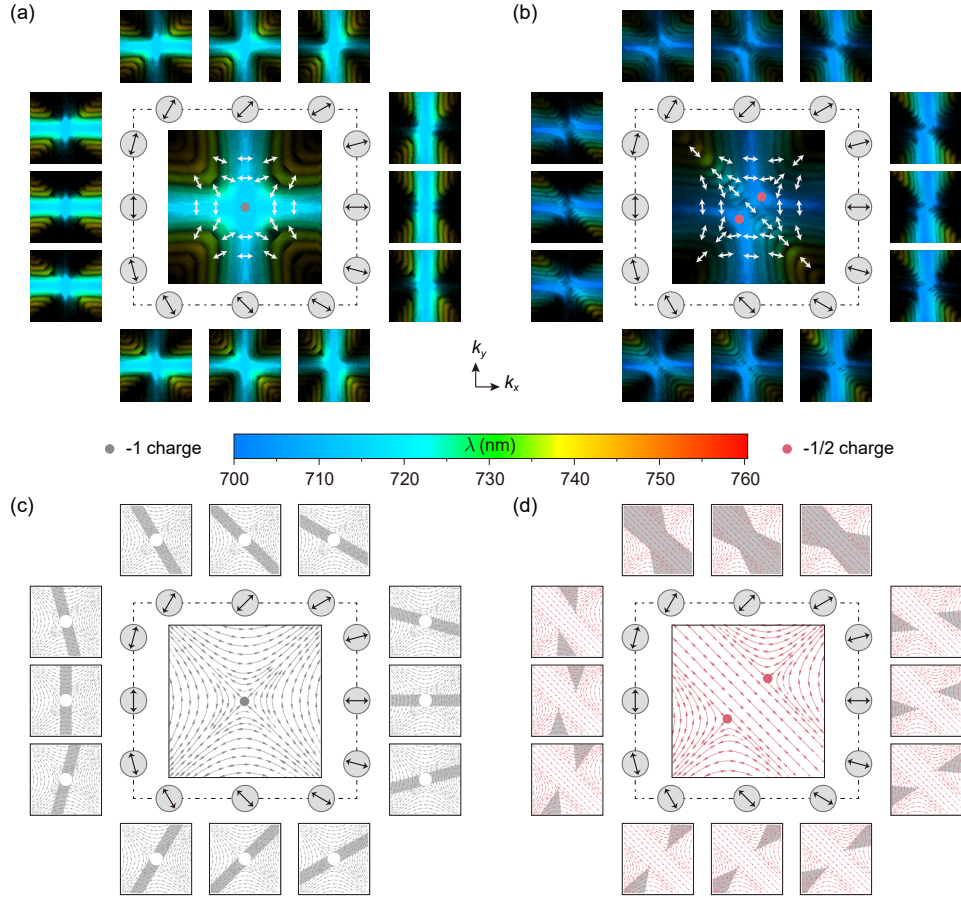


Figure S6: Extinction map of the bands without the mark lines for (a)  $C_{4v}$  and (b)  $C_{2v}$  structures. We also give schematic views showing spinning dark patterns for (c)  $C_{4v}$  and (d)  $C_{2v}$  structures. To mimic the experiment, the regions wherein polarization vectors are from 70 to 110 degrees to the direction of the polarizer are shown as the dark patterns corresponding to that where signals diminish in (a) and (b).

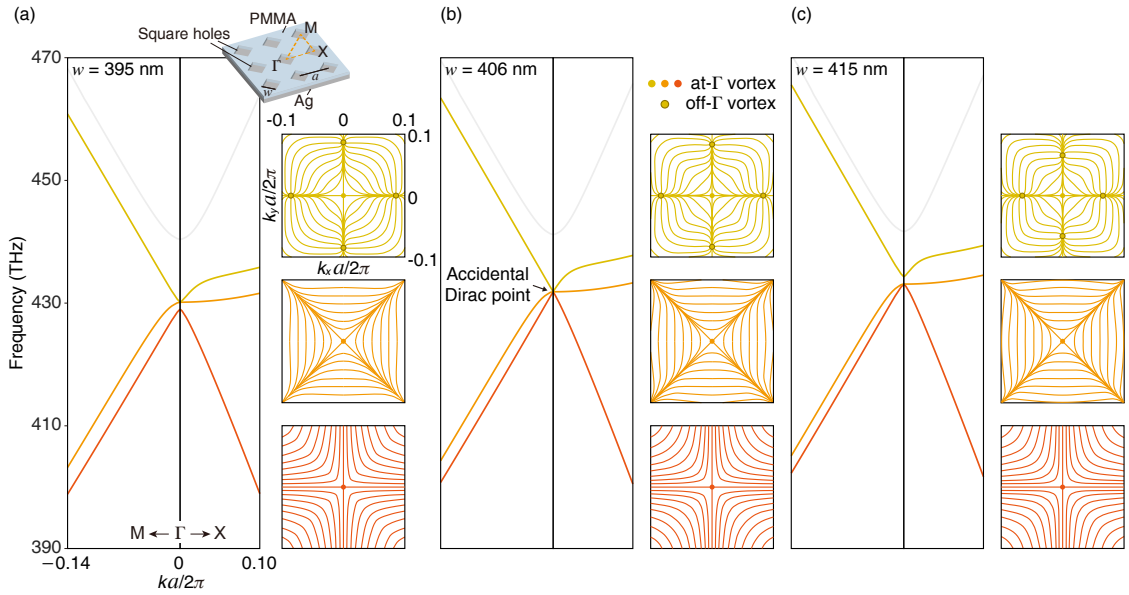


Figure S7: Band structures and corresponding polarization maps of plasmonic crystals with different side lengths: (a) 395 nm, (b) 406 nm and (c) 415 nm. Band TM2, TM3 and TM4 are marked with red, orange and yellow. The polarization maps corresponding to different bands are marked with the same colors as the bands. The vortex polarization singularities are marked as dots. Inset of (a): the schematic view of the structures.